INITIAL RESULTS FROM A TRACKING RECEIVER DIRECTION FINDER FOR WHISTLER MODE SIGNALS

M. K. Leavitt, D. L. Carpenter, N. T. Seely, R. R. Padden, and J. H. Doolittle

Radioscience Laboratory, Stanford University, Stanford, California 94305

Abstract. A new apparatus combining a tracking receiver and a direction-finding signal processor for observation of VLF whistler mode signals is described. The system is expected to achieve greater bearing accuracy than can be obtained from a conventional goniometer and is usable on a wider variety of signals than can be processed by most other techniques. Convenience in data output has been emphasized. In July-August 1975 the new tracker/direction finder (TR/DF) was successfully field tested at Roberval, Canada ($L \simeq 4$). Observations were made on natural whistlers and emissions and on signals from the Siple, Antarctica, VLF transmitter. As a test of accuracy on arrival bearing of whistler mode signals, the TR/DF output was compared with results from a goniometer operating from the same set of crossed loop and vertical antennas. The two systems agreed within $\simeq 10°$ on several-minute averages of bearings of both Siple transmitter pulses and natural signals. Effects of multipath propagation and polarization error have been identified. On the basis of the initial data sets it is found that whistler mode signal paths in the outer plasmasphere have ionospheric exit points that can frequently be resolved to within a region 30-40 km on a side. The apparent whistler mode signal path endpoints are relatively close to the ionospheric projections of the field lines along which the wave energy propagated, within 50-100 km (in the north-south direction). Bearings of Siple transmitter signals show an apparent concentration to the southwest of the receiving station.

Introduction

Magnetospheric whistler mode signals observed on the ground are often relatively narrow band and tend to rise or fall in frequency with characteristic periods that range from fractions of a second to several seconds. The waves are evidently guided or 'ducted' down to some upper ionospheric height between 200 and 3000 km, after which the propagation is controlled by the regular ionospheric density structure. Following penetration of the ionosphere, the energy propagates radially outward in the earth-ionosphere wave guide in a normal transverse electromagnetic mode (for reviews of whistler mode propagation, see Helliwell [1965] and Walker [1976]). By determining the azimuthal direction of arrival of this signal received at several spaced ground sites the duct exit point can theoretically be located.

In conventional dispersion analysis of broadband whistler and VLF emission records, only the propagation path latitude or equatorial radius is determined with accuracy. This places important limits on studies of magnetospheric density gradients and of longitudinal motions of the plasma. Direction finding of duct exit points should help to avoid these limits and should also provide new information on the propagation characteristics of magnetospheric ducts. Furthermore, direction finding in real time may contribute to the success of balloon, rocket, and satellite experiments in which VLF wave activity is of interest. The purpose of this paper is to describe a new type of tracking receiver/direction finder developed at Stanford University by one of the present authors [Leavitt, 1975].

Direction finding (DF) techniques originally developed for subionospheric signals have been applied to whistler mode waves with some success. Crary [1961], Watts [1959], and Bullough and Sagredo [1973] have reported the use of goniometers. These devices electronically synthesize a rotating loop antenna pattern by combining the outputs from a fixed pair of crossed loop antennas. The goniometer output over the entire VLF band is recorded and then spectrum analyzed onto a film strip. An observer must then measure the times of occurrence of intensity nulls in the signal trace to determine the direction of arrival. The duration of the signal must be greater than the goniometer rotational period (typically 1/20 s), and the rotational period must in turn be long in comparison with the inverse bandwidth of the spectrum-analyzing filter. Another limitation of the goniometer is its susceptibility to 'polarization error' for incident waves which are elliptically polarized.

Delloue [1960] has reported a quite different approach to DF which compares the signal phase between spaced antennas and which is not subject to polarization error. However, the long wavelengths of VLF signals dictate antenna spacings of the order of kilometers, with attendant costs in installation, maintenance, and transmission of the signals to a central point for processing.

Systems designed to cope with the polarization and elevation angle characteristics of whistler mode waves have been described by Cousins [1972] and Tsuruda and Hayashi [1974]. These experimenters have augmented the crossed loops with a vertical electric antenna. Cousins has shown that there are several different equations for DF which combine the vertical signal with the loop signals to reduce polarization error. Using a computer to process digitized audio records, he applied each of these techniques and compared the results. The computational power and time required to analyze each 1.2-s record, however, has precluded the practical development of this approach. The Tsuruda and Hayashi apparatus implements one particular DF equation in real time using analog filtering and multiplication. The equation chosen promises to yield zero polarization error for elliptically polarized waves. However, it does not allow the equipment to respond to purely vertically polarized signals, a feature which precludes calibration and testing using the many ground wave signals available from existing transmitters. Also, since the filtering is narrow in bandwidth, the apparatus cannot extract complete data from whistler mode signals with wide frequency excursions unless the

Paper number 7A1036.
0148-0227/78/047A-1036$03.00

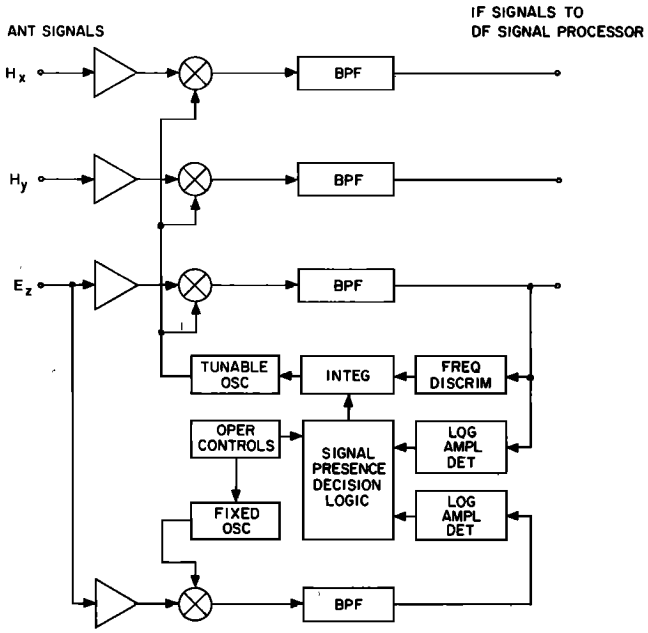

Fig. 1. Tracking receiver block diagram.

three antenna signals are recorded and repeatedly played back with successive adjustments to the filter frequency.

Description of the Apparatus

The approach described here couples a frequency tracking receiver (TR) to a DF signal processor. The tracking receiver captures and follows the frequency excursions of whistler mode signals in real time, producing outputs which are translated and filtered replicas of the antenna signals. An analog processor operates on these outputs to determine the direction of arrival using one of the DF equations. The particular equation chosen yields lower polarization error than the goniometer on whistler mode waves yet retains the ability to respond to ground wave signals. The system outputs are available both in real time, for on-site inspection, and in tape-recorded form. A detailed description of the apparatus has been provided by Leavitt [1975].

Tracking Receiver

A block diagram of the tracking receiver is presented in Figure 1. The primary function of translating and filtering the antenna signals is accomplished by a three-channel superheterodyne receiver with a common electronically tunable local oscillator. The IF signal from one channel is applied to a frequency discriminator to provide an error signal for frequency tracking and to a logarithmic amplitude detector for measurement of signal strength. Frequency tracking is accomplished by feeding back the frequency error signal through an integrator to control the tunable local oscillator. Inclusion of the integrator makes it possible to track frequency excursions over the entire VLF range when it is necessary. When no signal is present, the integrator is disabled and the received frequency is fixed. When a signal is detected, the integrator is enabled and the frequency of the signal is tracked. The method by which signal presence is determined is explained in the next paragraph.

The VLF noise background in which whistler mode signals are immersed consists of both relatively constant 'white' noise and highly impulsive noise bursts generated by local thunderstorm activity. Generally, the whistler mode signals are stronger than the constant noise, so that a fixed amplitude threshold would be adequate to detect signal presence. However, the impulsive noise bursts are often stronger than the whistler mode signals and would cause a great deal of false triggering. To reduce this problem, the apparatus includes an auxiliary receiver channel tuned to a higher frequency at which few whistler mode signals are encountered but which still contains energy from the impulsive noise. The presence of a desired signal is declared only when the main receiver channel amplitude exceeds both a preset absolute threshold and a varying threshold which follows the noise amplitude in the auxiliary channel.

Another problem is the presence of interference in the form of discrete spectral lines. Some of these signals originate from the VLF communications/navigation transmitters, while others represent induction fields from local power distribution systems or magnetospheric line spectra that originate in radiation from power grids [Helliwell et al., 1975]. To counteract the tendency of the TR to lock onto these signals, controls are provided to set limits on the frequency range in the tracking mode and also the time duration of the tracking period.

The task of the operator in setting up the TR/DF apparatus is primarily one of selecting the initial receiving frequency of the TR and then adjusting the amplitude thresholds so that the equipment is operating as sensitively as possible without excessive false triggering. The setting of limits on the tracking frequency range

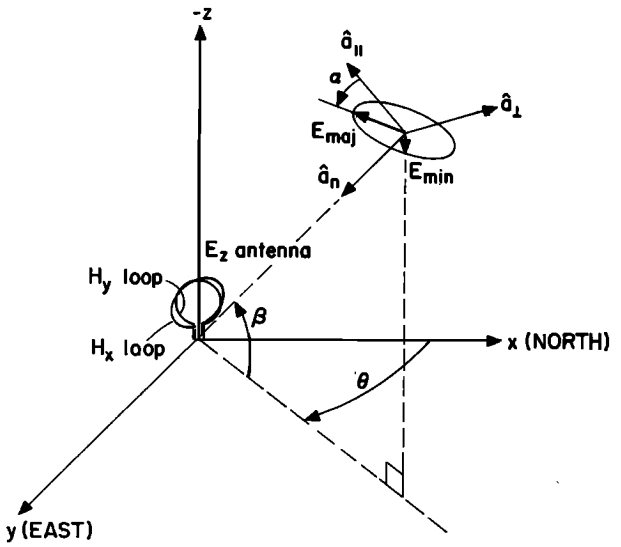

Fig. 2. Parameters of general plane wave incident on a direction finder site. Here, $\hat{a}_n$, $\hat{a}_{\parallel}$ and $\hat{a}_{\perp}$ are the unit vectors in the wave coordinate system; $\hat{a}_n$ is the direction of propagation, $\hat{a}_{\parallel}$ lies in the plane of incidence, and $\hat{a}_{\perp}$ is mutually perpendicular to $\hat{a}_n$ and $\hat{a}_{\parallel}$.

and time duration may be required if the interference described in the preceding paragraph is encountered. After these initial adjustments are accomplished, operation of the apparatus is automatic.

The design characteristics of the TR may be summarized as follows.

Frequency coverage	0.5-10, 10-20 kHz
IF output frequency	6 kHz $\pm$ 170 Hz
IF filter bandwidth	340 Hz
Dynamic range	60 dB
Frequency tracking ability	>50 kHz/sec

Note that a narrow IF bandwidth could be employed, but only if it is accompanied by a reduction in the frequency-tracking loop gain to maintain stability. This in turn limits the maximum tracking rate (df/dt). The resultant relationship between bandwidth and maximum tracking rate is

$$df/dt_{max} \simeq \frac{BW_{IF}^2}{2} \qquad (1)$$

DF Signal Processor

Our analysis of the DF signal processing begins with the definition of a general plane wave incident on a DF site (Figure 2). The major and minor semiaxes of the polarization ellipse are E_{maj} and E_{min}, and their ratio E_{min}/E_{maj} is denoted by R. The tilt angle of the major axis relative to the wave plane of incidence is α. The direction from which the wave is arriving is defined by an azimuth θ and an elevation β.

The crossed loops and vertical antenna system sense field components H_x, H_y, and E_z. For the general wave defined above, these components are ($e^{j\omega t}$ being assumed)

$$\begin{aligned} H_x &= \frac{1}{\eta} E_{maj}[(\cos\alpha - jR\sin\alpha)(\sin\theta) \\ &\quad + (\sin\alpha + jR\cos\alpha)(-\sin\beta\cos\theta)] \\ H_y &= \frac{1}{\eta} E_{maj}[(\cos\alpha - jR\sin\alpha)(-\cos\theta) \\ &\quad + (\sin\alpha + jR\cos\alpha)(-\sin\beta\sin\theta)] \\ E_z &= E_{maj}[(\cos\alpha - jR\sin\alpha)(-\cos\beta)] \end{aligned} \qquad (2)$$

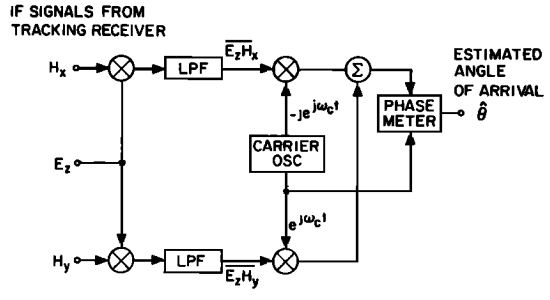

Fig. 3. Analog DF signal processor.

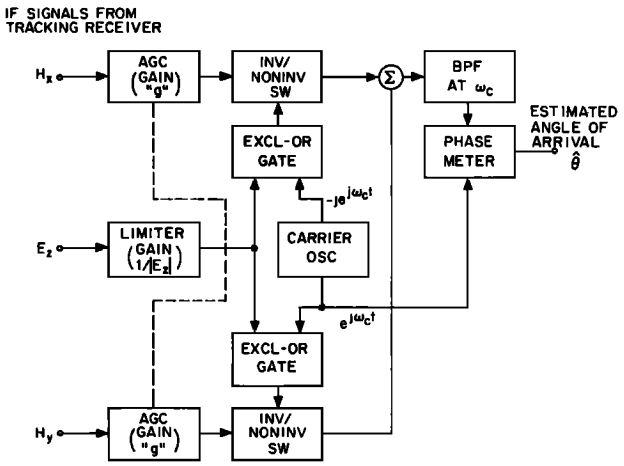

Fig. 4. Modified implementation of DF signal processor.

Operating on IF replicas of these components, the DF signal processor provides an estimate $\hat{\theta}$ of the azimuthal direction of arrival using the following equation (overbars denote time-averaged quantities):

$$\hat{\theta} = \arg\left[\overline{E_zH_y} - j\,\overline{E_zH_x}\right] \qquad (3)$$

The response of the direction finder to any given incident wave may be computed by substituting (2) in (3), yielding

$$\begin{aligned} \hat{\theta} &= \arg\left[(\cos^2\alpha + R^2\sin^2\alpha)e^{j\theta}\right. \\ &\quad \left. + \cos\alpha\sin\alpha\sin\beta(R^2-1)e^{j(\theta+\pi/2)}\right] \end{aligned} \qquad (4)$$

This result has intentionally been arranged into vector components at angles θ and $\theta+\pi/2$. The first component is a desired response, producing $\hat{\theta}$ equal to θ, whereas the second component is the origin of 'polarization error' which causes $\hat{\theta}$ to deviate from θ. The error $\Delta\theta$ is given by

$$\Delta\theta = \arctan\left[\frac{\cos\alpha\sin\alpha\sin\beta(R^2-1)}{\cos^2\alpha + R^2\sin^2\alpha}\right] \qquad (5)$$

Equation (5) demonstrates that for signals of low elevation angle ($\beta \simeq 0$) or nearly pure circular polarization ($R \simeq 1$) the error tends to zero. Furthermore, even for elliptically polarized signals ($R \neq 1$) the error tends to zero for ellipse orientations α near 0° or 90°. In comparison, the polarization error of a goniometer tends to zero only for low elevation angles ($\beta \simeq 0$) or pure linear polarization in the plane of incidence ($R \simeq 0$ and $\alpha \simeq 0$ simultaneously).

A straightforward analog implementation of (3) is illustrated by Figure 3. The crossmultiplications and low-pass filtering generate signals corresponding to $\overline{E_zH_x}$ and $\overline{E_zH_y}$. These signals modulate phase quadrature carrier waves at frequency ω_c. The sum of the two modulated carriers is $(\overline{E_zH_y} - j\,\overline{E_zH_x})e^{j\omega_c t}$, which is compared in phase to the reference carrier $e^{j\omega_c t}$. The measured phase difference corresponds to the angle of arrival $\hat{\theta}$ in (3).

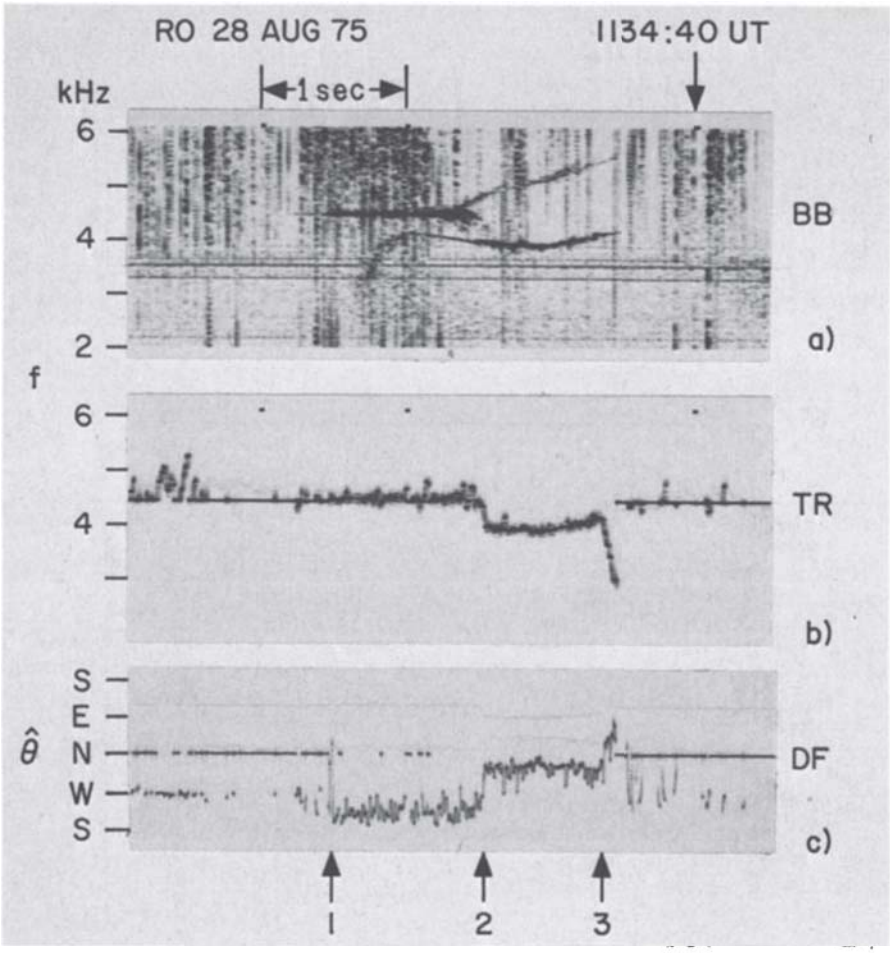

Fig. 5. Examples of spectrographic displays of data acquired by the TR/DF during field tests at Roberval, Canada. (a) Broadband record showing Siple transmitter pulse near 4.5 kHz. Below the Siple pulse is a noise event triggered by the upper part of a whistler. (b) Replica of the passband center frequency of the tracking receiver. (c) Signal bearing information. The bearing indication was automatically reset to north when the receiver was not in the tracking mode. The horizontal lines near 3 kHz in Figure 5a represent interference from the local power system.

A modified implementation shown in Figure 4 has been chosen for the apparatus to eliminate the need for analog multipliers and to provide a wide dynamic range. The H_x and H_y signals are amplified by automatic gain control circuits which are ganged together so that the amplitude ratio of the signals is preserved. The E_z signal is amplitude limited to convert it to a binary square wave. Products are formed between this binary signal and square wave equivalents of the quadrature carriers by digital exclusive-or gates. Multiplications of the resulting binary signals by the H_x and H_y signals are accomplished with analog invert/noninvert switches. After summing, a band-pass filter at ω_c removes the harmonics introduced by the square waves, leaving a signal $(g/|E_z|)\ (\overline{E_z H_y} - j\ \overline{E_z H_x})\ e^{j\omega_c t}$. The phase of this signal, which is unaffected by the amplitude term $g/|E_z|$, corresponds to $\hat{\theta}$ just as it did in the analog implementation of Figure 3.

Data Display and Recording

The direction-of-arrival data and signal parameters of interest (frequency, signal strength, and signal-to-noise ratio) are made available for display on a panel meter, digital readout, or external analog chart recorder. In addition, the frequency, direction of arrival, and either signal strength or signal-to-noise ratio are converted to a frequency modulation format. The FM carriers are combined into a single audio channel and recorded on a track adjacent to a recording of the broadband VLF spectrum which served as input to the TR/DF system.

Spectrograms of data recorded in this mode during field tests of the TR/DF at Roberval, Canada are shown in Figure 5. Figure 5a shows the broadband spectrum from 2 to 6 kHz versus time. There are two prominent signals on the record, a Siple transmitter pulse at 4.5 kHz that is followed by a rising, triggered noise and a noise event that develops below the Siple pulse. The noise event begins as the upper part of a nose whistler and continues as a triggered noise near 4 kHz. Figure 5b shows the FM carrier representing the passband center frequency of the tracking receiver; that frequency was reset to 4.5 kHz when the receiver was not in the tracking mode. Near the beginning of the record the TR was briefly activated by several lightning-induced spherics. Between times t_1 and t_2 (indicated below

Figure 5c) the TR followed the Siple transmitter signal, while between t_2 and t_3 it tracked the noise triggered by the whistler. Figure 5a shows the FM carrier containing information on bearing (with respect to the geomagnetically aligned loop antennas). Note that the bearing indication was automatically reset to north when the receiver was not in the tracking mode. The spheric activity, the Siple pulse, and the whistler-triggered emission all exhibit well-defined and measurably different bearings.

In some cases it is desirable to postanalyze the data by recording the broadband spectra from all three antennas and processing the data through the TR/DF at the home laboratory. In this mode it is possible to vary the tracking parameters as desired and thus to investigate features of the data that were missed during the real-time field operation. Postanalysis has been performed on several data sets acquired during the June-August 1975 Roberval campaign. In cases for which multipath effects and polarization error do not appear to be serious the data replicate well the information recorded in the field. Bearings on known VLF transmitters are within about 5° of those determined from the DF carrier recorded in the field, while bearings on whistler mode signals are within less than 10° of the field values. The greater discrepancy on whistler mode signals is introduced because channel-to-channel phase variations in the tape-recording process reduce the polarization error immunity of the DF technique.

Expected Limitations on DF Accuracy

The accuracy of the DF signal-processing circuitry under laboratory conditions has been measured at 1.25°rms. However, the limitations to DF accuracy on real received signals are set by polarization error, noise, interference, and multiple incident ray conditions.

Polarization error cannot be precisely predicted by using (5) because the polarization ellipse of real received whistler mode signals is unknown. However, it is possible to formulate general hypotheses separating favorable from adverse conditions as follows.

1. Distant duct exit points may be expected to produce a dominant low-elevation angle ray. For this condition the polarization error will be small.

2. Closer duct exit points may be expected to produce a circularly polarized high-elevation angle direct ray. If the reflection coefficients of ground and ionosphere are low, the direct ray will dominate and polarization error will be low or moderate.

3. The combination of very low close duct exit points and high ground and ionospheric reflection coefficients may be expected to produce a multiple ray situation with an unpredictable composite polarization ellipse. Polarization error may be substantial. Because the composite polarization ellipse will vary as the relative phases of the multiple rays change, the polarization error would be expected to vary with signal frequency. Such a variation in the bearing data would be an indication of high polarization error conditions. Averaging of data over time and frequency may reduce this error as described by Crary [1961].

The effects of noise and directional interference have been analyzed by Leavitt [1975]. In following his analysis the presence of a nondirectional noise power N in the IF passband accompanying a signal power of S produces a mean square fluctuation in the angle indication given by

$$\overline{\Delta\theta^2_{rad}} \simeq \frac{1}{2(S/N)} \tag{6}$$

Time averaging of the angle indication occurs both in the apparatus and in the examination of recorded data, reducing this error. For a sample case of 20 dB S/N and 0.1-s averaging, the resultant rms error is approximately 0.7°.

The effects of directional interference cannot be eliminated by time averaging because a bias error is produced in addition to a fluctuating error component. For an interference power I with an arrival angle displaced by θ_d from the desired signal this bias is approximated by

$$\overline{\Delta\theta_{rad}} \simeq \frac{\sin\theta_d}{2(S/I)} \tag{7}$$

For example, an interfering signal displaced by 90° and 10 dB below the desired signal produces a DF error of approximately 3°.

The discussion above also applies to situations where multiple ray paths exist. Because whistler mode signals vary in frequency over

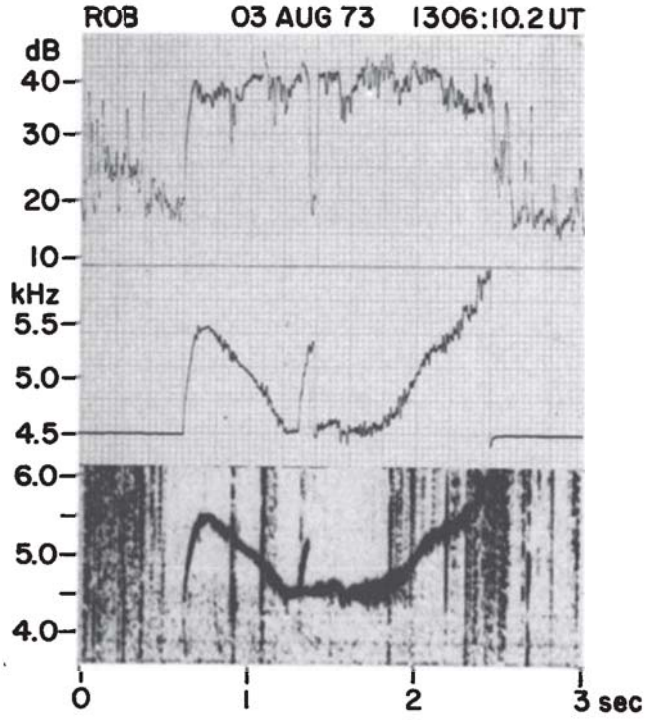

Fig. 6. Illustration of use of the TR/DF as a laboratory tracking instrument. (Top) Log amplitude within the 340-Hz tracking passband. (Middle) Replica of tracker passband center frequency. (Bottom) Broadband VLF spectrum of a narrow-band noise event initiated by the upper part of a natural whistler.

TABLE 1. Direction-Finding Results on VLF Stations Received at Roberval, Quebec

Station	Frequency	Location	Indicated Bearing, deg.	Corrected Bearing, deg.	True Bearing, deg.	Error, deg.
GBR	16.0	England	74.3	56.0	56.8	-0.8
NPG	18.6	Washington	307.5	289.7	288.7	+1.0
OMEGA/NOR	10.2	Norway	53.4	34.3	34.3	0.0
OMEGA/TRI	10.2	Trinidad	189.7	169.0	163.0	+6.8
OMEGA/H.	10.2	Hawaii	297.9	280.3	281.1	-0.8
OMEGA/N.D.	10.2	N. Dakota	286.2	268.6	273.1	-4.5

time, multiple rays arriving via different paths with differing delays are generally offset in frequency. The angle indication produced by the apparatus under these conditions will show periodic or noiselike fluctuations; the average value of $\hat{\theta}$ will tend to indicate the strongest ray but may be biased by the weaker rays following (7).

Tests of System Performance

Tracking Ability

The receiver has proved successful in tracking most of the known features of whistlers, Siple transmitter signals, and VLF emissions. It has in fact been used as a laboratory tracking instrument for cases in which information on the instantaneous amplitude of a narrow-band signal is desired. Results of such an application are shown in Figure 6. The spectrum in the bottom panel contains the upper, rising part of two nose whistlers ($t \approx 0.7$ and 1.3 s)

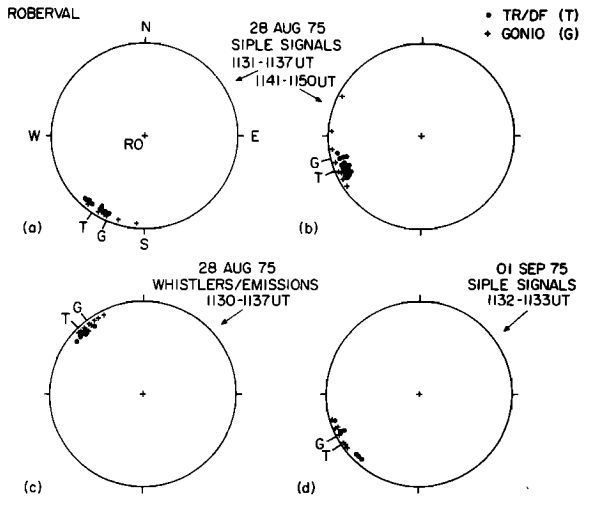

Fig. 7. Comparison of results on arrival bearing of signals processed by the TR/DF and by a goniometer operating from the same crossed loops and vertical antennas. (a and b) Tracker and goniometer bearings of Siple signals during two periods on August 28, 1975. (c) Tracker and goniometer bearings of whistlers and whistler-triggered emissions on August 28, 1975. (d) Tracker and goniometer bearings of Siple signals on September 1, 1975.

as well as an intense, narrow-band emission triggered by the first whistler. A recording of this spectrum was presented to the TR, which was tuned to 4.5 kHz, as is indicated by the tracking frequency replica in the middle panel. The tracker readily followed the ≈15-kHz/s variation of the two whistlers. The signal strength in the tracker passband, shown on a log scale in the upper panel, is relatively constant during the event. The amount of hunting or fluctuation in the tracking frequency varies with time (compare, for example, conditions at $t \approx 1$ s and at $t = 1.7$ s), apparently because of variations in the coherence of the signal being tracked. Amplitude-frequency displays of this kind are being used in current studies of wave-wave interactions in the magnetosphere.

DF Accuracy

Wave guide signals. During the June-August 1975 field tests at Roberval, Canada, bearing data were taken on stations NPG, GBR, and four Omega stations. Table 1 summarizes the results. The 'indicated bearings' are with reference to the magnetic field orientation of the crossed loop antennas. The 'corrected bearings' transform the indicated bearings into geographic coordinates. The 'true bearing' is the calculated great circle bearing. Bearings on the VLF stations were found to be accurate within a few degrees and highly repeatable from day to day.

Whistler mode signals. The positions of whistler mode signal path endpoints in the ionosphere are not known a priori; the accuracy of bearings on such signals must be assessed indirectly. One such assessment was made through a comparison of the output of the TR/DF with results from a goniometer designed and built at Stanford by E. Paschal (unpublished notes, 1975). The TR/DF and goniometer operated from the same crossed loop and vertical antennas. The addition of the electric antenna removed the 180° ambiguity that would otherwise be present in the goniometer output.

Data from the two available cases of simultaneous TR/DF and goniometer operation are illustrated in Figure 7. Figures 7a, 7b, and 7d represent Siple signals, while Figure 7c shows results on whistlers and associated triggered emissions. The TR/DF results are shown by solid circles, and the goniometer data by pluses. Each circle or plus represents an average over the ≈1-s duration of a whistler

event or of an individual Siple pulse or other transmitted segment (see Figure 5). For the goniometer, eight individual measurements typically were made per case; for the TR/DF the number was usually larger because of the essentially continuous nature of the system's DF output. Roughly half the events were analyzed by one system only; some events were 'missed' by the TR/DF, while in some cases of successful TR/DF operation the goniometer information was insufficient in duration or poorly defined.

The intervals represented in Figure 7 were ones of relatively steady bearings. Symbols T and G denote averages over the interval for the TR/DF and the goniometer, respectively; these several-minute averages agree within less than 10°. This is excellent agreement; ±10° is roughly the uncertainty in determining a reference direction during scaling of goniometer data from spectrograms.

Polarization Error

Polarization error has been tentatively identified in a number of the data sets acquired. As was expected (see earlier notes), it is characterized by relatively smooth variations in apparent bearing with frequency. The frequency-tracking properties of the TR/DF system facilitate recognition of this effect. Figure 8 shows an example from the July-August 1975 Roberval campaign. The upper panel contains broadband spectra of three rising frequency ramps transmitted from Siple. The middle panel shows the broadband data and tracking frequency superposed, while the lower panel provides DF and signal strength information. During tracking of the three ramps the bearings move more or less steadily from east of north to west of north. This pattern persisted for several minutes. In pronounced cases of the type illustrated, the bearing shift was about 40° over 400 Hz or approximately 0.1°/Hz.

While much remains to be learned about polarization error, its adverse effects can be partially overcome by restricting measurements to the frequent intervals in which variations in bearing with frequency are relatively small (as demonstrated by DF on variable frequency signals). Averaging of bearings over frequency can also be employed; bearing-versus-frequency signatures such as those illustrated in Figure 8 have been observed to change substantially on a time scale of several minutes while the average bearing over the bandwidth of the signal remained relatively well behaved [Leavitt, 1975].

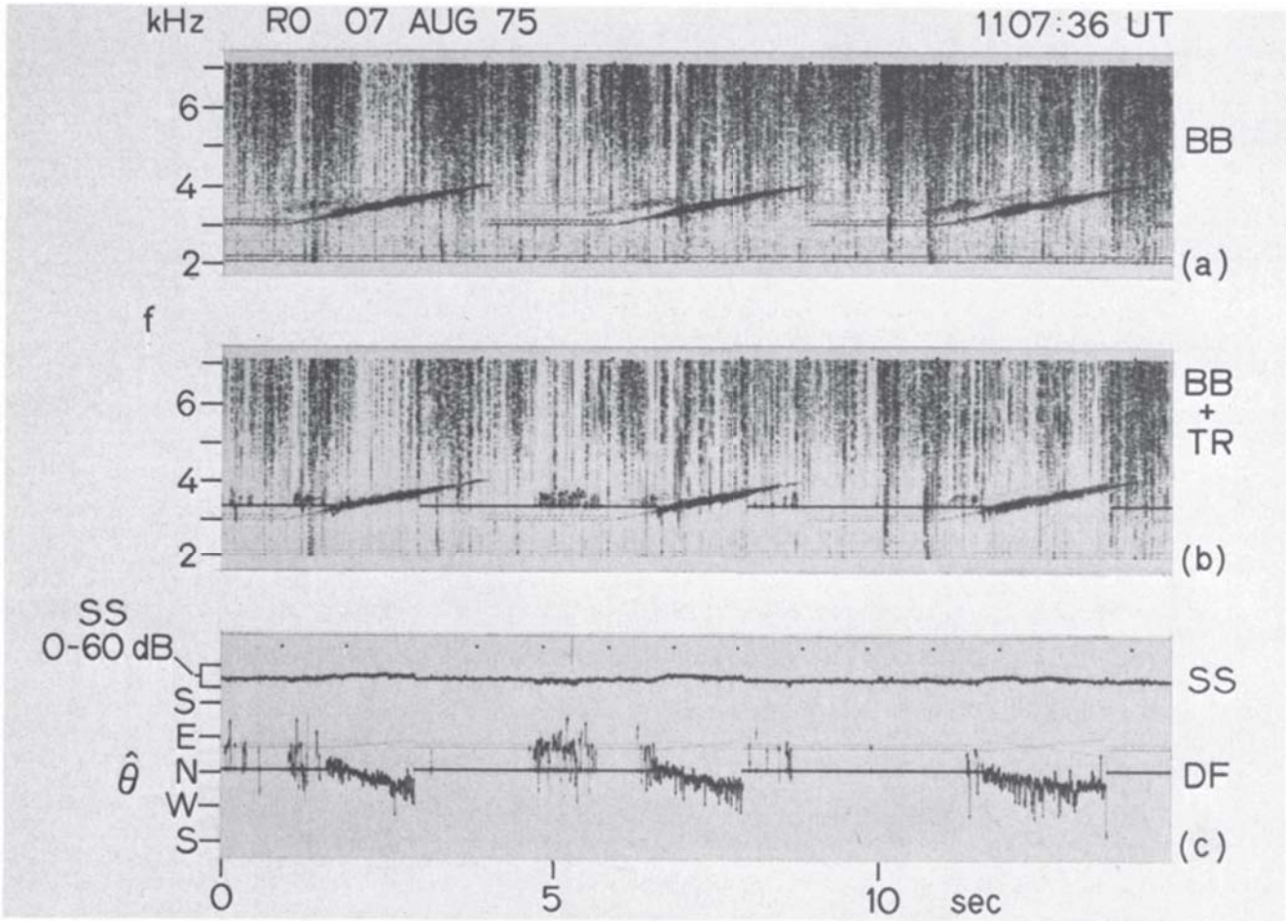

Fig. 8. Spectrographic illustration of TR/DF operation under conditions of apparent polarization error. (a) Broadband records of Siple transmitter signals. (b) The broadband data of Figure 8a with the passband center frequency of the TR/DF superposed. (c) Log signal strength within the tracker passband (above) and DF angle (below).

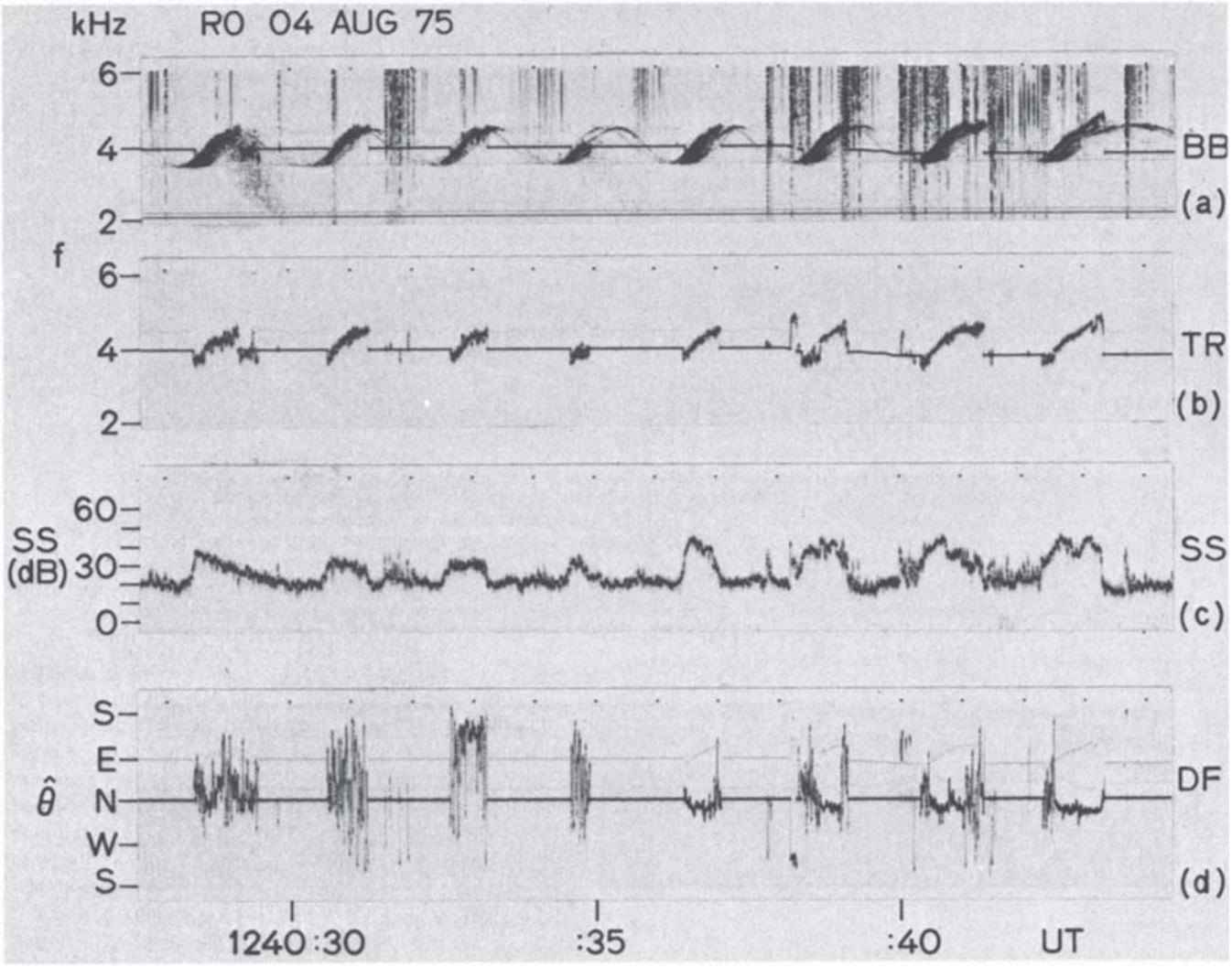

Fig. 9. Spectrographic illustration of effects of multipath signals on TR/DF output. (a) Broadband VLF recording of Siple signals sinusoidally varying in frequency. The tracker center frequency is superposed. Near t = 1240:39 there were small adjustments in tracker frequency by the field operator. (b) Replica of the tracker passband center frequency. (c) Log signal strength within the tracker passband. (d) Direction finder output.

Multipath Effects

In general, whistlers and transmitter signals propagate on multiple paths, and there is overlap of the received signals in the frequency-time domain. Strategies for avoiding adverse effects of multipath propagation on TR/DF results include transmission of frequency ramps, tracking on triggered emissions that become isolated in frequency and time, and tracking during intervals when the signal output of a single path is exceptionally intense.

When frequency ramps (or similar continuous forms with $df/dt \neq 0$) propagate on several paths, they are received with time separations that depend on the distribution in L value of the paths and on the magnetospheric electron density distribution. Depending on the value of df/dt and the travel time separations, the tracker may or may not include more than one path component in its 340-Hz passband at a given time.

Figure 9 illustrates a TR/DF analysis of Siple transmitter signals that display strong multipath effects. The upper panel shows the received broadband spectra with the tracking frequency superposed. Eight sinusoidal frequency variations with a period of 2 s were transmitted. The received spectra contain closely spaced multipath components; the overall travel time spread is ≈0.4 s.

The problems of multipath and the benefits of tracking on an exceptionally intense signal are illustrated in Figures 9b, 9c, and 9d, which show a replica of the tracker frequency, signal strength in the tracker passband, and the signal bearing, respectively. During tracking of the first four sinusoids the tracker frequency fluctuated rapidly as it followed the general trend of the signal. The bearing information is relatively noisy and variable from case to case, apparently as a result of differences in the structure of the successive events and hence in the path in frequency-time space followed by the tracker.

The results from the last four sinusoids are substantially different. An intense component containing some irregular frequency variations

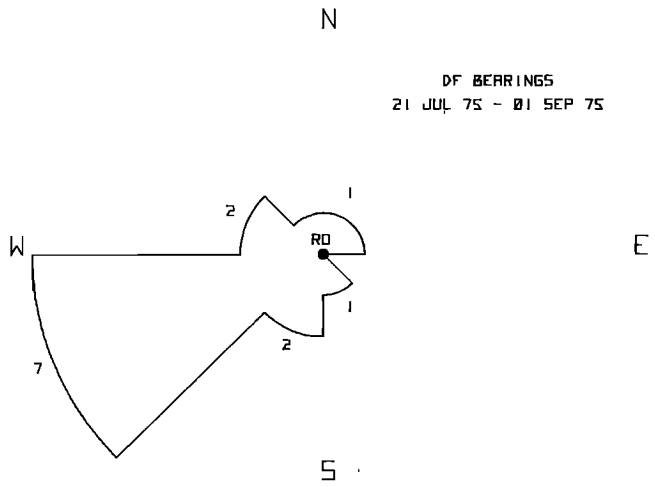

Fig. 10. Polar histogram of Siple signal bearings representing 15 hours of data from 10 observing days in July-September 1975.

appeared at the leading edge of each event. The tracker followed this component, which was about 10 dB stronger (see Figure 9c) than the signals previously tracked. The tracking frequency signature (Figure 9b) became narrow in bandwidth, and the DF signatures became relatively well defined and repeatable from event to event. The noisier parts of the last four DF signatures correspond to periods either when df/dt was relatively small, additional multipath elements thus being brought within the tracker passband, or when the components within the passband were of roughly comparable intensity. Note the lack of apparent polarization error in the DF signature for the eighth event; the tracker frequency changed by ≈1 kHz while the bearing remained nearly constant.

Experimental Results

While the TR/DF data available are not extensive, they suggest the following conclusions.

1. Whistler mode signal paths in the outer plasmasphere have ionospheric exit points that can frequently be resolved to within a region 30-40 km on a side. Figure 5 illustrates a case of this kind; an average bearing for the Siple pulse (t_1 to t_2) and for the whistler-triggered emission (t_2 to t_3) can be scaled to within ≈10°. Averaging over results for several pulses, as is shown in Figure 7, suggests that bearings can be resolved to within an arc of ≈15°. By taking a typical exit point range of 150 km (see below) this corresponds to a region of dimension ≈30-40 km on a side.

2. The apparent whistler mode signal path endpoints are relatively close to the ionospheric projections of the field lines along which the wave energy propagated, within 50-100 km (in the north-south direction). The ducting process along field lines in the magnetosphere may be expected to trap waves efficiently down to some upper ionospheric height, after which ionospheric gradients control the propagation [e.g., Helliwell, 1965; Walker, 1976]. It is important to know the extent of deviation of the waves from the downward projection of the duct, for example, as part of wave-particle interaction and precipitation experiments.

Whistler dispersion analysis, following the methods of Carpenter and Miller [1976], was used to determine the equatorial radius of propagation paths during the DF experiments. A realistic geomagnetic field model was then employed to identify curves at ionospheric height corresponding to constant values of equatorial radius near the longitude of Roberval. Intersection of these curves and observed directions of signal arrival provides a crude means of triangulation on signal path exit points. Frequent lack of successful triangulation, such as occurs in cases of equatorial radius curve to the north and bearing to the south, would imply large deviations of the waves from the field lines. In fact, the triangulation was possible in a large fraction of the cases, a result suggesting that the deviation is not usually greater than 100 km. Details of this analysis are presented by Seely [1977].

3. Bearings on whistler mode signal path endpoints can undergo relatively rapid shifts. Figures 7a and 7b represent such a case; they show Siple signal bearings during two intervals separated by about 4 min. During the 4-min separation the bearings appeared to shift continuously in direction. There was also a small, few-percent shift in travel time during this period. It is not known whether the shift represented a fast bulk flow or whether it was due to temporal changes in polarization error, in duct fine structure, or in the ionospheric segment of the propagation path. Further applications of direction finding, particularly from spaced locations, should permit identification of the factors involved in such shifts.

4. From earlier dispersion analysis it was inferred that the Siple signal path endpoints are relatively close to Roberval, Canada, within approximately ±200 km in the north-south direction [Carpenter and Miller, 1976]. The triangulation method described above was applied to all of the cases in which dispersion analysis could be applied. The majority of the observed cases were found to have endpoints within less than 200 km of the observing station, a typical value being 150 km. Seely [1977] presents additional detail on this point.

5. Bearings of Siple transmitter signals show an apparent concentration to the southwest. It was found that within almost every observing hour there were periods of several minutes when relatively well behaved, repeatable bearings could be obtained and during which multipath effects and polarization error were at a relative minimum and/or signal-to-noise ratio was at a maximum. Bearings for these times were scaled; roughly 15 hours of data from 10 observing days were included in the analysis. The observed bearings were found to concentrate in the southwest. This is illustrated by the polar histogram in Figure 10. The concentration may be related to the fact that the calculated geomagnetic conjugate point of the ionospheric region of maximum illumination of the Siple transmitter is ≈35 km southwest of Roberval [Seely, 1977].

Discussion and Concluding Remarks

While the data in hand are limited in extent, they may help to resolve certain questions recently raised about whistler mode propagation to ground points. For example, it was suggested by Morgan [1976] that plasmaspheric whistler ducts may be elongated in the generally east-west sense or in the direction of magnetospheric plasma flow. Our results suggest that this is not the case. Many path endpoints have been resolved to within a region of dimension 30-40 km on a side.

We find that the TR/DF system is an effective tool for direction finding and believe that it will provide a basis for real-time assessment of wave activity during future experiments. While the system confirms ideas on plasmaspheric propagation, it also reveals a great complexity in the wave environment in terms of temporal and spatial variation in wave parameters. Substantial further application of DF techniques will probably be required in order to document these complexities properly.

With the aid of dispersion analysis and information on typical duct endpoint distance from a ground station it should be possible to use the TR/DF to advantage at a single site. However, relatively long campaigns are required in order to obtain cases in which the effects of interest are clearly displayed. Crossed bearing analysis from two or more sites is clearly needed as a means of extending the area covered and improving the accuracy of path endpoint information. DF from two sites will be attempted in the Roberval area in 1978. Work of this kind is already being carried out using goniometers at Antarctic stations as part of IMS research activities.

Acknowledgements. We thank R. A. Helliwell and C. G. Park for support and guidance and J. P. Katsufrakis for management of the field programs in which the data were acquired. We are grateful to E. Paschal, who designed and built the goniometer used in this research, and to J. Billey, who carried out a demanding program of data acquisition during the 1975 Roberval campaign. This research was supported in part by the Atmospheric Sciences Section of the National Science Foundation under grant ATM75-15852 and grant DES75-07707, in part by the Division of Polar Programs under grant GV-41369X, and in part by the Office of Naval Research under contract NONR N00014-76-C-0689.

The editor thanks K. Bullough for his assistance in evaluating this paper.

References

Bullough, K., and J. L. Sagredo, VLF goniometer observations at Halley Bay, Antarctica, I. The equipment and the measurement of signal bearing, Planet. Space Sci., 21, 899, 1973.

Carpenter, D. L., and T. R. Miller, Ducted magnetospheric propagation of signals from the Siple, Antarctica, VLF transmitter, J. Geophys. Res., 81, 2692, 1976.

Cousins, M. D., Direction finding on whistlers and related VLF signals, Tech. Rep. 3432-2, Radioscience Lab., Stanford Electron. Lab., Stanford Univ., Stanford, Calif., 1972.

Crary, J. H., The effect of the earth-ionosphere waveguide on whistlers, Tech. Rep. 9, Radioscience Lab., Stanford Electron. Lab., Stanford Univ., Stanford, Calif., 1961.

Delloue, J., La determination de la direction d'arrivée et de la polarisation des atmosphériques siffleurs, 1, J. Phys. Radium, 6, 514, 1960.

Helliwell, R. A., Whistlers and Related Ionospheric Phenomena, Stanford University Press, Stanford, Calif., 1965.

Helliwell, R. A., J. P. Katsufrakis, T. F. Bell, and R. Raghuram, VLF line radiation in the earth's magnetosphere and its association with power system radiation, J. Geophys. Res., 80, 4249, 1975.

Leavitt, M. K., A frequency-tracking direction finder for whistlers and other very low frequency signals, Tech. Rep. 3456-2, Radioscience Lab., Stanford Electron. Lab., Stanford Univ., Stanford, Calif., 1975.

Morgan, M. G., Simultaneous observation of whistlers at two $L \simeq 4$ Alaskan stations, J. Geophys. Res., 81, 3977, 1976.

Seely, N. T., Whistler propagation in a distorted quiettime model magnetosphere, Tech. Rep. 3472-1, Radioscience Lab., Stanford Electron. Lab., Stanford Univ., Stanford, Calif., 1977.

Tsuruda, K., and K. Hayashi, A new method for direction finding of elliptically polarized VLF waves, Rep. 509, Inst. of Space and Aerosp. Sci., Univ. of Tokyo, 1974.

Walker, A. D. M., The theory of whistler propagation, Rev. Geophys. Space Phys., 14, (4), 629, 1976.

Watts, J. M., Direction findings on whistlers, J. Geophys. Res., 64, 2029, 1959.

(Received July 2, 1977;
accepted November 2, 1977.)